Resting-State Functional Connectivity by Independent Component Analysis-Based Markers Corresponds to Areas of Initial Seizure Propagation Established by Prior Modalities from the Hypothalamus

Varina L. Boerwinkle,[1] Angus A. Wilfong,[1] and Daniel J. Curry[2]

Abstract

The aims of this study were to evaluate a clinically practical functional connectivity (fc) protocol designed to blindly identify the corresponding areas of initial seizure propagation and also to differentiate these areas from remote secondary areas affected by seizure. The patients in this cohort had intractable epilepsy caused by intrahypothalamic hamartoma, which is the location of the ictal focus. The ictal propagation pathway is homogeneous and established, thus creating the optimum situation for the proposed method validation study. Twelve patients with seizures from hypothalamic hamartoma and six normal control patients underwent resting-state functional MRI, using independent component analysis (ICA) to identify network differences in patients. This was followed by seed-based connectivity measures to determine the extent of fc derangement between hypothalamus and these areas. The areas with significant change in connectivity were compared with the results of prior studies' modalities used to evaluate seizure propagation. The left amygdala-parahippocampal gyrus area, cingulate gyrus, and occipitotemporal gyrus demonstrated the highest derangement in connectivity with the hypothalamus, $p < 0.01$, corresponding to the initial seizure propagation areas established by prior modalities. Areas of secondary ictal propagation were differentiated from these initial locations by first being identified as an abnormal neuronal signal source through ICA, but did not show significant connectivity directly with the known ictal focus. Noninvasive connectivity measures correspond to areas of initial ictal propagation and differentiate such areas from secondary ictal propagation, which may aid in ictal focus surgical disconnection planning and support the use of this newer modality for adjunctive information in epilepsy surgery evaluation.

Keywords: functional connectivity; independent component analysis; pediatric epilepsy; resting-state functional connectivity magnetic resonance imaging; seizure localization

Introduction

FUNCTIONAL CONNECTIVITY (fc) based markers in epilepsy are evolving toward clinical utility. Simultaneous electrocorticography and functional MRI (EEG-fMRI) demonstrate the capacity of fc measures to detect and localize epileptogenic events (Gotman and Pittau, 2011). These studies have shown ictal propagation pathways, but are limited thus far to patients who happen to have epileptogenic events during the scan and also those with clear plausible prior hypothesis of the pathway. Even then, at best, EEG-fMRI can only help discern between pathways examined, of which all could possibly be incorrect, or clinically impractical to discern in most individuals with epilepsy (Murta et al., 2012).

A step forward from simultaneous event-containing EEG-fMRI studies is epileptogenic-event-negative EEG-fMRI studies. This technique has shown the effectiveness of resting-state (rs) fc measures to localize previously known ictal foci by identifying the areas of maximal connectivity derangement in overlapping blood oxygen level dependent (BOLD) signal sources in the absence of epileptogenic events (Hunyadi et al., 2013).

[1]Department of Pediatric Neurology, Texas Children's Hospital, Baylor College of Medicine, Houston, Texas.
[2]Department of Neurosurgery, Texas Children's Hospital, Baylor College of Medicine, Houston, Texas.

A next logical concern is the ability of fc measures alone to discriminate reliably between areas of local initial ictal propagation from those of further remote propagation or distant network connectivity changes. Rs-fc measures in temporal lobe epilepsy have begun to show the difference between initial and distant locations of ictal propagation (Morgan et al., 2015). Fc measures inside of the ictal focus are significantly reduced, whereas fc measures in secondary propagation areas are significantly increased. The distant regions involved in secondary epileptogenesis show disrupted connectivity with no reported relationship to the ictal driver or ictal propagation pathway. In Morgan's hypothesis-driven study, the regions of previously known ictal propagation, by prior methods, were the only regions examined for changes in fc measures over time. Hence, it remains unknown if fc-measure-identified areas without prior hypothesis-driven search in a cortex-wide-blinded, data-driven evaluation would be the same as those identified by proven modalities.

Propagation of electrical phenomenon in the brain occurs on a millisecond basis, and modalities measuring at this time scale are traditionally used, with exceptions such as single-photon emission computed tomography (SPECT) and positron emission tomography (PET). As with PET (Rastogi et al., 2008), rs-fMRI is not measured on a millisecond basis but rather every 2 sec. Similarly to the metabolic measure of PET, the underlying pathology of the epilepsy may still significantly affect fc measures in a localizing manner.

To be clear, this study did not focus on localizing the source of seizure (as already shown by Hunyadi) nor on differentiating the seizure source from initial areas of propagation. Rather, the aim was to determine if rs-fMRI alone can blindly identify previously known areas of the initial seizure propagation pathway and also to differentiate these initial areas from those shown to be more remote in the ictal propagation pathway or network connectivity changes, which are not shown to be part of the seizure propagation pathway. The utility of such information is translatable to surgical planning for disconnecting the known ictal focus from its connections to the rest of the brain to stop seizure propagation and simultaneously reduce the degree of invasiveness and potential loss of function induced by the procedure. In addition, convergent localizing information from a completely separate additional noninvasive modality measured on an individual basis is desirable before brain surgery.

A uniquely poised clinical population to examine this hypothesis are those with epilepsy due to intra-hypothalamic hamartoma (HH), because the location of the seizure focus and propagation pathway are homogeneous and established, creating the opportunity to validate rs-fMRI. Intrahypothalamic hamartomas are benign neuronal overgrowths consistently associated with intractable epilepsy. Seizures associated with HH are generated from within the HH itself (Kuzniecky et al., 1997).

Unlike cortical structures, which may have connections broadly over the brain through the centrum semiovale and many other white matter tracts, the hypothalamus has limited connections from which seizure can propagate. The hypothalamus is connected to the rest of the brain primarily through two major white matter tracts. The first is the mammillothalamic tract, which starts at the hypothalamus/mammillary body, then extends to the anterior nucleus of the thalamus, followed by connections to the cingulate gyrus. The second is the for-

nix, which connects the hypothalamus to the hippocampus (Baroncini et al., 2012). And there are some smaller connecting fibers from the hypothalamus to the ventral septum and the nucleus retroambiguus within the pons (Lauterbach et al., 2013).

Ictal propagation from the hypothalamus has been studied using EEG-fMRI (Kokkinos et al., 2012; Leal et al., 2009), intraoperative depth electrode (Nguyen et al., 2003), and ictal SPECT (Kuzniecky et al., 1997). The most detailed evidence of the pathway is from simultaneous EEG-fMRI capturing about 60 seizures in one individual (Leal et al., 2009). In this study, the signal started in the HH, traveled to the left hippocampus and mesial-occipital lobe, and then to the left cingulate and dorsolateral frontal lobe. Another patient had ictal EEG-fMRI capturing 21 seizures, with increased BOLD in the precuneus, anterior cingulate, and medial-occipital areas (Kokkinos et al., 2012). These findings have been verified by intraoperative EEG (Nguyen et al., 2003) and ictal SPECT (Kuzniecky et al., 1997). As three separate methods have identified the same few well-localized areas of ictal propagation from HH, this population serves as a good pilot population to evaluate the use of fc measures to blindly identify and differentiate remote from initial propagation areas when the ictal driver is fairly established.

Methods

Rather than assuming areas of hypothalamic-induced dysfunction or seizure propagation, we used a blinded approach. Thus, all major brain networks were queried for differences between those with HH and normal controls. We started with independent component analysis (ICA) to derive the whole-brain rs networks across all subjects (Step 1). The networks detected by ICA are well established (Smith et al., 2009), reliably found in all ages from 30 weeks gestation (Doria et al., 2010), and are stable across populations (Damoiseaux et al., 2006). Next, using the dual regression approach (Filippini et al., 2009) and permutation testing (Nichols and Holmes, 2002), we determined networks, which differed between the groups (Step 2).

Finally, these target areas of major cortical network differences were tested for correlation strength with the hypothalamus in a voxel-wise approach known as seed-based partial correlation analysis and compared between groups using randomization (Step 3) (Smith and Nichols, 2008). This approach has been used previously in both healthy and diseased states (Delnooz et al., 2015; O'Reilly et al., 2010; Zarei et al., 2012).

Subjects

Twelve HH patients and six healthy controls, with groups proportionally matched for age and gender, were evaluated (Table 1; also see Supplementary Fig. S1 [Supplementary Data are available online at www.liebertpub.com/brain] for subject HH anatomic images). Note that given the age spread, care was taken to use age-matched standard brain atlases for coregistration, before registration to the group standard.

Two subjects and two controls were not sedated, as this is standard clinical practice in cooperative individuals. The level of light conscious sedation with propofol has shown to not interfere with large-scale connectivity detection (Marcar et al., 2006; Tagliazucchi et al., 2015; Vanderby et al., 2010). All patients were being treated for HH-associated

TABLE 1. TABULATED SUBJECT INFORMATION

Age (years)	Onset age	Gender	IQ or DQ	Sedated	Handedness	MRI	Prior surgery
HH							
2.3	4 months	M	80	Yes	Nonhanded	Right	
3.1	Early infancy	M	80	Yes	L (familial)	Right	
3.7	3.3 years	M	100	Yes	R	Right	
3.7	1 month	M	95	Yes	R	Right	
3.8	3 months	F	75	Yes	R	Right	
6.0	12 months	F	50	Yes	nonhanded	Left	
9.4	17 months	M	100	Yes	L	Left	Transcallosal ablation
9.6	"early infancy"	M	116	Yes	R	Left	Laser ablation
10.0	"early infancy"	M	88	Yes	R	Right	
10.0	6 weeks	M	114	Yes	R	Left	
15.6	"early infancy"	M	97	No	L (familial)	Right	Gamma knife
20.0	7 months	F	100	No	R	Right	
Controls							
2.1		M	100	Yes	R	Normal	
2.1		M	100	Yes	R	Normal	
2.9		F	100	Yes	L	Normal	
3.7		M	130	Yes	R	Normal	
19.0		M	137	No	R	Normal	
21.0		F	135	No	R	Normal	

No significant difference was found in patient characteristics across groups, except developmental quotient, by t-test, $p = 0.0074$. Hypothalamic hamartoma (HH) patients' average age was 8.4 years, and the control group 8.4 years. Female-to-male ratios were 1:4 and 1:3, respectively. MRI HH hemispheric laterality is listed by dominant side of the connection between the HH and the hypothalamus.

intractable epilepsy by the center's pediatric epilepsy specialists, and the MRI with resting state data was collected as part of routine care.

The local bioethics committee and hospital administration approved acquisition of rs-fMRI as part of the presurgical epilepsy evaluation. Three of the subject group had prior surgery with no lasting change in gelastic seizure control. Four of the neurodevelopmentally normal controls had been recruited as part of a separate local ethics committee-approved autism-related study on a highly limited basis from families affected by autism, whose parents gave informed consent for sedated rs-fMRI. Specifically, as part of the Baylor IRB H-25894, the control group of children will "have a clinical indication for brain MRI independent of the study," be "solicited through siblings of autistic children," or "be identified by study personnel from the TCH MRI schedule or patients getting brain MRI." The other two controls were nonsedated volunteers just over the age of 18 years, who underwent MRI for the purpose of machine and protocol evaluation. These two controls were recruited to increase the control group's age range and sedation state to more closely resemble the patient group. All subjects' consent complies with the Declaration of Helsinki.

Image acquisition and preprocessing

Images were acquired on a 3 Tesla MRI (Ingenuity, Philips Medical Systems, Best, the Netherlands) equipped with a 32-channel head coil. Ten of 12 patients' and 4 of 6 controls' scans were obtained under light conscious sedation with propofol. Propofol at levels producing conscious sedation reduces the BOLD signal strength by $\sim 10\%$, still allowing for network detection (Schrouff et al., 2011; Vanderby et al., 2010).

Rs-fMRI parameters included TR 2000 msec, TE 30 msec, matrix size 80×80, flip angle $80°$, number of slices 46, slice

thickness 3.4 mm with no gap [similar to other recent studies of deep gray matter (Toulmin et al., 2015)], and in plane resolution 3×3 mm, and the number of total volumes was 600. Rs-fMRI scan time was 20 min, far exceeding the accepted minimum required for analysis (Damoiseaux et al., 2006). For anatomic reference, a T1W whole-brain sequence was obtained with TR 9 msec, TE 4 msec, flip angle $8°$, slice thickness 0.9 mm, and in plane resolution 0.9×0.9 mm. Anatomical images were reviewed by an experienced neuroradiologist.

Preprocessing and analysis

Analysis was carried out using the FSL suite of fMRI processing tool, MELODIC (Beckmann and Smith, 2004). Standard preprocessing steps were applied as such: the first five volumes were deleted to allow for T1 saturation, high pass filter 100 sec, interleaved slice time correction, spatial smoothing 1 mm (lower than typical 2–3 mm; smoothing was incorporated, as the thickness of the hypothalamus, 2–3 mm, could blur into ventricles and nearby arteries), and motion corrected using MCFLIRT (Jenkinson et al., 2002), with nonbrain structures removed. All subjects had less than 1 mm motion, the majority being less than 0.5 mm greatest displacement in any direction.

Individual functional scans were first registered to the subject's high resolution anatomical scan using linear registration (Jenkinson and Smith, 2001) and then optimized using boundary-based registration (Greve and Fischl, 2009). Individual's anatomical scans were then registered to a group standard brain (MNI T1 2 mm template), again using FNIRT (Jenkinson et al., 2012). For children less than 5 years of age, an additional registration of the subject's anatomical scan was performed to an age-matched anatomical template (Fonov et al., 2011) and this template was registered to a common template.

Step 1. Whole-brain fcMRI networks determined for all subjects. From the functional data, group-level networks were derived using ICA (Beckmann and Smith, 2004). Rs data are a series of pictures of the brain, like a movie, one image taken every 2 sec. MRI parameters are set to maximize the image contrast created by different levels of oxygen content throughout the brain tissue, known as the BOLD signal. Both neuronal and non-neuronal signal sources contribute to the variation in BOLD signal between the series of images. The objective is to separate out the neuronal signal sources of interest from all the other sources, based on signature characteristics.

ICA is designed to separate out signal sources, which regularly oscillate over time (time course) in a spatially independent manner from other signal sources. The time courses modeled are spatially independent, but this type of analysis allows a single area of the brain to belong to more than one component. This is important, as it is known that a given area of brain tissue can participate in more than one network. The results of ICA are a set of spatial maps or components, one for each signal source (an example of signal source with further explanation is given in the Supplementary Fig. S2).

As the sampling rate of fcMRI is every 2 sec and ictal spread occurs over milliseconds of time, the results of fcMRI analysis cannot show the millisecond phenomenon changes, but instead may show more lasting resultant changes in local brain function. Each resultant component has identifiable traits, which allow neuronal versus noise categorization. For example, the internal carotid artery pulsates in sync with the cardiac rhythm and is located centrally at the base of the brain, whereas the primary visual network oscillates much slower and is located in the occipital lobe. Automated categorization paradigms have not yet been tested on populations with epilepsy.

To perform group analysis, each subject's total rs signal variation is used to normalize the respective dataset, thus reducing the possibility that any one individual's preprocessed signal variation dominates the group results. Next, these individual datasets are concatenated together across time, and ICA is performed. The number of signal sources modeled was based on an automated dimensionality estimate using a Bayesian approach, which determines the dimensionality of a dataset by maximizing the differences between the Gaussian and non-Gaussian signal sources with nonoverlapping time courses (Beckmann et al., 2005). ICA maps were thresholded using an alternative hypothesis test based on fitting a Gaussian/Gamma mixture model to the distribution of voxel intensities within spatial maps and controlling the local false discovery rate at $p < 0.05$ (Beckmann et al., 2005).

Step 2. Network differences between patients and controls. To determine significant differences in networks between the HH patients and the control group, the individual's networks and their time courses were first derived using dual regression (Filippini et al., 2009). This was done by regressing the time course of each group-derived component into each subject's preprocessed rs dataset, thereby identifying the set of time courses for each subject, which corresponded to the group-derived time courses.

This set of individual time courses was then regressed into the same individual preprocessed fc-data, yielding the subject-specific spatial maps. Finally, the subject's network images were compared for significant differences across the group using nonparametric permutation testing (5000 permutations per network) with threshold-free cluster enhancement and correction for multiple comparisons (Smith and Nichols, 2008). This allowed identification of areas of abnormality in the group of HH patients, which became the hypothesized candidates corresponding to the previously identified areas of initial seizure propagation by querying their functional relationship to the hypothalamus in the subsequent analysis step.
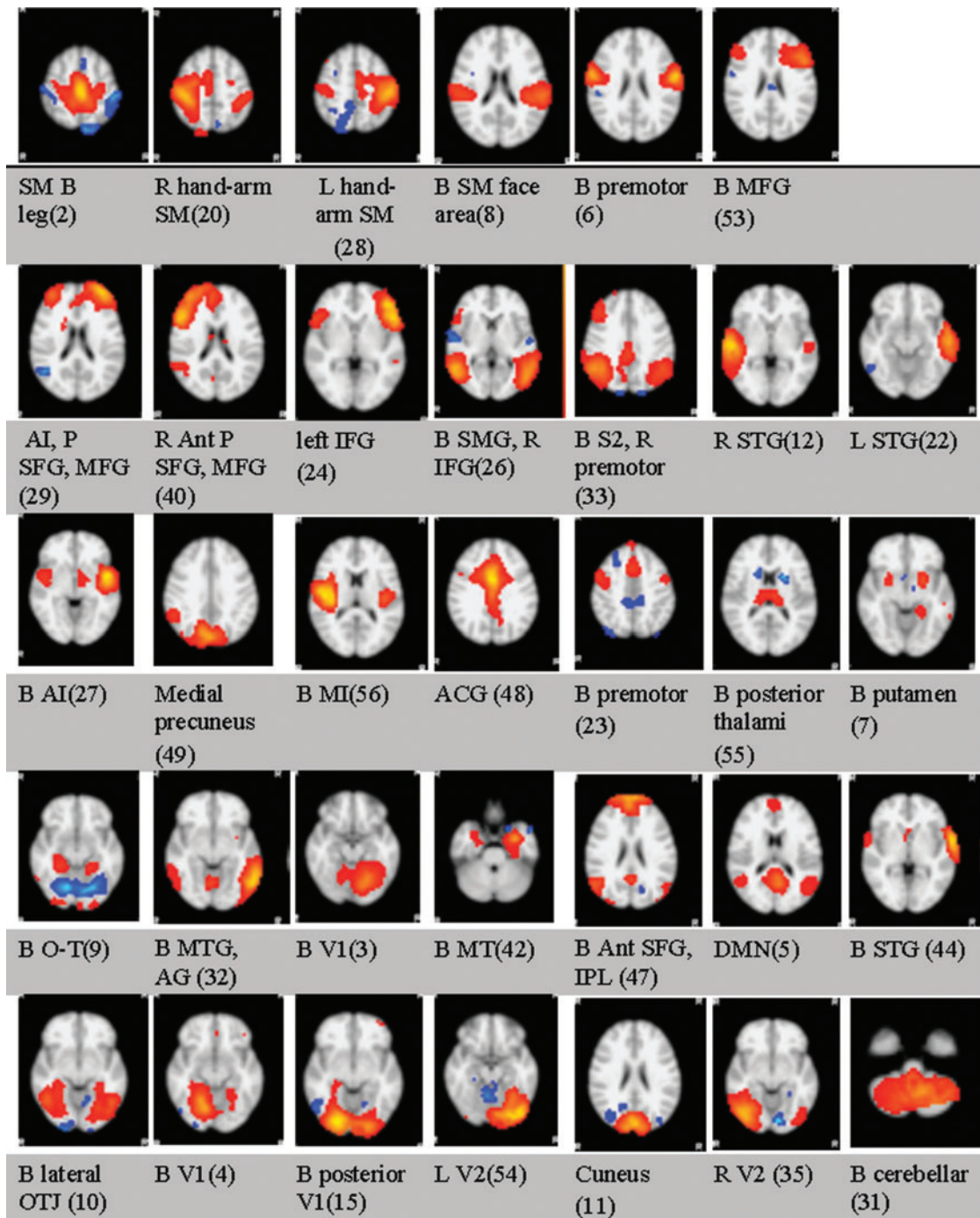
Step 3. Connectivity measure between HH and abnormal areas identified by step 2. The purpose of step 3 was to determine if areas of major difference in whole-brain networks identified in step 2 actually had significant differences in connectivity directly with the hypothalamus itself. The seed-based correlation analysis (SBCA) (O'Reilly et al., 2010) was aimed to determine which, if any, of these areas are linked to the dysfunction of the hypothalamus, to be defined as significant fc differences versus indirect effects of the dysfunction predicted to not show significant differences in the SBCA.

To answer this question, each target area was independently queried for its connectivity to the hypothalamus, while regressing out the time series of all other areas, using SBCA, similar to Toulmin's method (Toulmin et al., 2015). SBCA was used to test the connectivity of every voxel in the hypothalamus with each of the identified components from step 2.

Accordingly, first a manually generated bilateral hypothalamic mask in standard and individual space was created (Supplementary Fig. S3A, B). Individual HH boundaries were visually inspected for overlap to the hypothalamic mask in standard space (Supplementary Fig. S3C). Given the bilateral neuronal connections within the hypothalamus, the bilateral HH mask was chosen, reducing the possibility of missed connectivity dysregulation from studying only the unilateral HH, and also most of the HH were asymmetrically bilaterally connected to the hypothalami. The bilateral hypothalamic standard mask minimized individual effects of anatomical distortion from the hamartoma on the hypothalamus, reducing possible effects from the wide variety of size, location, and prior surgery. In addition, this strategy was selected because internal HH connectivity was not the effect of interest, but rather the focus was the effect on the hypothalamus in relation to the cortical targets.

SBCA was performed for each subject with regression of known confounders modeled in the individual (Toulmin et al., 2015), including time series of individual white matter, cerebrospinal fluid in ventricles, and head motion. The results were subject-specific hypothalamic spatial masks consisting of partial correlation values for each of the significant components identified by ICA with Randomise (Smith and Nichols, 2008).

Next, to compare across groups, the subject partial correlation maps were normalized by r-to-z Fisher's transform. Finally, to determine which components partial correlation z-score maps were significantly different between HH and control groups, the maps were subjected to nonparametric permutation testing (using Randomise with 5000 permutations and threshold-free cluster enhancement) (Smith and Nichols, 2008).

SM B leg(2)	R hand-arm SM(20)	L hand-arm SM (28)	B SM face area(8)	B premotor (6)	B MFG (53)
AI, P SFG, MFG (29)	R Ant P SFG, MFG (40)	left IFG (24)	B SMG, R IFG(26)	B S2, R premotor (33)	R STG(12) · L STG(22)
B AI(27)	Medial precuneus (49)	B MI(56)	ACG (48)	B premotor (23)	B posterior thalami (55) · B putamen (7)
B O-T(9)	B MTG, AG (32)	B V1(3)	B MT(42)	B Ant SFG, IPL (47)	DMN(5) · B STG (44)
B lateral OTJ (10)	B V1(4)	B posterior V1(15)	L V2(54)	Cuneus (11)	R V2 (35) · B cerebellar (31)

FIG. 1. Large-scale ICA-derived brain networks of all subjects. Results from Step 1 (Supplementary Data for full set of the resultant images): For all subjects, including both groups, whole-brain networks are overlaid on the MRI152 template. They are, as described by the primary areas of location, the bilateral sensory-motor leg area, right sensory-motor arm-hand area, left sensory-motor arm-hand area, bilateral sensory-motor face area, bilateral premotor, bilateral middle frontal gyrus, bilateral anterior insula with prefrontal superior and middle frontal gyrus, right anterior prefrontal superior and middle frontal gyrus, left inferior frontal gyrus, bilateral supramarginal gyrus and right inferior frontal gyrus, bilateral lateral secondary sensory parietal areas and right premotor cortex, right superior temporal gyrus, left superior temporal gyrus, bilateral anterior insula, medial precuneus, bilateral medial insula, anterior cingulate gyrus, bilateral premotor, bilateral posterior thalami, bilateral putamen, bilateral occipitotemporal gyrus, bilateral middle temporal and angular gyri, bilateral (L>R) primary visual cortex, bilateral mesial temporal cortex, bilateral anterior superior frontal gyri and inferior parietal lobules, default mode network, bilateral superior temporal gyri, bilateral lateral occipitotemporal lobe junction, bilateral (R>L) primary visual cortex, bilateral posterior primary visual cortex, left secondary visual association cortex, bilateral cuneus, right secondary visual cortex, and bilateral cerebellar. Ant, anterior; ACG, anterior cingulate gyrus; AG, angular gyrus; AI, anterior insula; B, bilateral; DMN, default mode network; ICA, independent component analysis; IFG, inferior frontal gyrus; IPL, inferior parietal lobule; L, left hemispheric; MI, medial insular; MFG, middle frontal gyrus; MT, mesial temporal; MTG, middle temporal gyrus; OTJ, occipitotemporal junction; P, prefrontal; PM, premotor area; R, right hemispheric; S2, secondary sensory association area; SFG, superior frontal gyrus; SM, sensory motor; SMG, supramarginal gyrus; STG, superior temporal gyrus; V1, primary visual cortex; V2, secondary visual association area.

Results

Step 1. Whole-brain fcMRI networks determined for all subjects

ICA revealed standard networks established by many other studies. There were a total of 67 detected signal sources, including signal sources from noise and actual networks. Thirty-four of the detected signal sources were neuronal networks, as determined by expert visual inspection to published norms (Fig. 1) (Beckmann et al., 2000; Damoiseaux et al., 2006; Smith et al., 2009).

Step 2. Network differences between patients and controls

Thirteen of the components from step 1 showed significantly increased fc in the subjects compared to controls, $p < 0.05$, corrected for multiple comparisons (Fig. 2).

Step 3. Connectivity measure between HH and abnormal areas identified by step 2

As shown in Table 2, 11 of 13 areas identified in step 2 demonstrated significantly increased connectivity with the hypothalamus, $p < 0.05$. All of the areas found to have significant connectivity derangement with the HH were the same as those previously found by other modalities to be areas of initial seizure propagation (Table 2). (The images in Table 2 are shown for visual inspection and for comparison to figures in other prior publications. The images are given in a larger version in Fig. 2, in which they are overlaid onto the standard brain image and subdivided by anatomic regions for viewing purposes.) Note that the left planum temporale and posterior thalamus listed in the last two rows of Table 2 were areas identified by step 2, but did not have a p-value demonstrating significant connectivity derangement with the hypothalamus itself and importantly were not areas of initial seizure propagation from other studies.
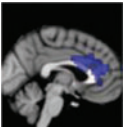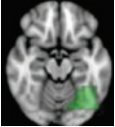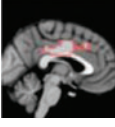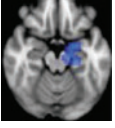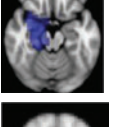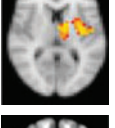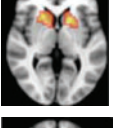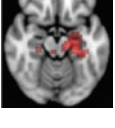
Discussion
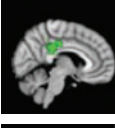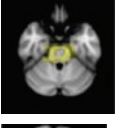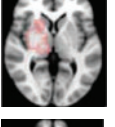
Areas of initial seizure propagation shown by other modalities correlated with the data-driven fc measures. The seizure propagation pathway was established by depth electrode (Kahane et al., 2003; Nguyen et al., 2003), fMRI-EEG (Kokkinos et al., 2012; Leal et al., 2009), and ictal SPECT-based (Kuzniecky et al., 1997) studies. These prior studies show that the areas with direct anatomical connection, along the Papez circuit through the hypothalamus' connection to the mammillothalamic tract and fornix, propagate the ictal activity first.

Then the ictal activity tracks to the next closest areas of the Papez circuit without direct anatomical connection to the HH and lastly to the most remote members of the circuit. The areas with significant maximal fc-measure difference are the same as those with the closest HH connection along the Papez circuit—the cingulate gyrus, hippocampus/mesial temporal/occipitotemporal junction area, and deep gray/thalamus (Kahane et al., 2003; Kokkinos et al., 2012; Kuzniecky et al., 1997; Leal et al., 2009; Nguyen et al., 2003). The other

Blue - L PHG, amygdala(43),
Red - L hippocampus(61),
Green - R amygdala(30),
Yellow – L OTG(54)

Blue – far anterior B ACG(63)
Pink - B medial ACG(48),
Green – PCG(33)

Yellow - PAG, NRA(21)

Green- NA, caudate(38)
Yellow- Medial thalami(55)

Red - L PT, SMG(8)

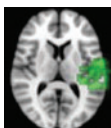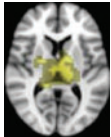Red - R putamen(34)
Green – L thalamus, operculum(7)
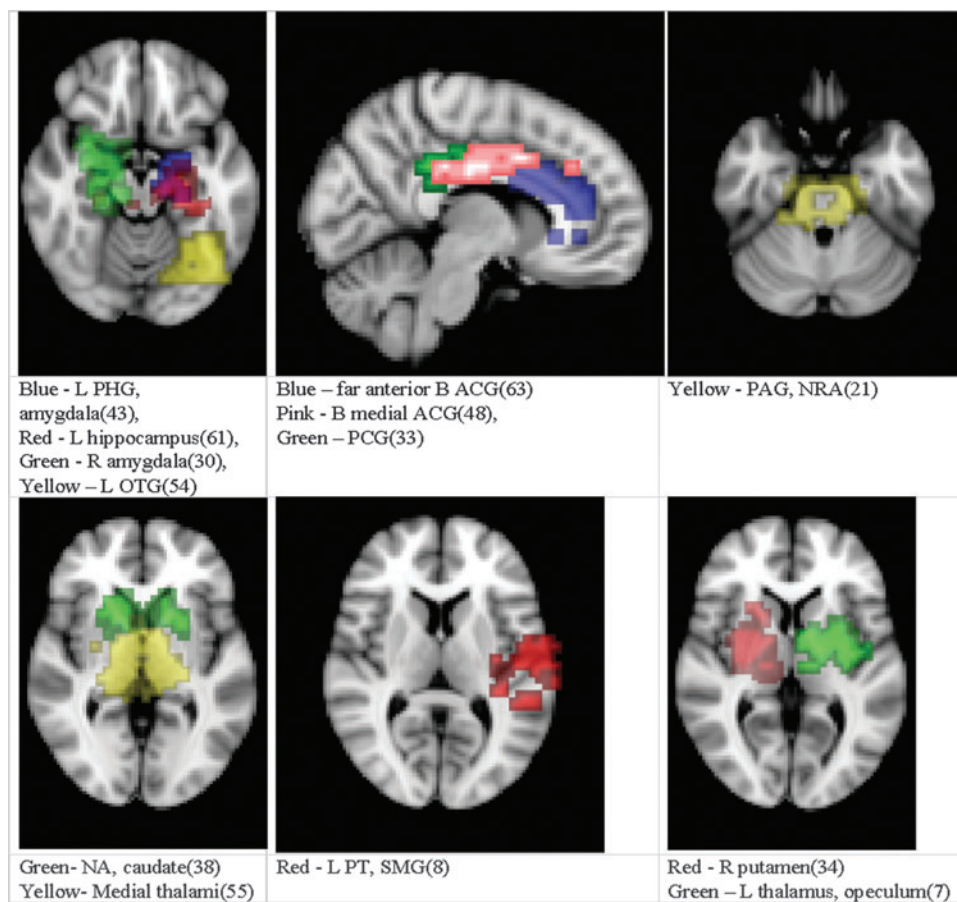
FIG. 2. Highest ICA-derived connectivity derangement in HH versus controls. Results from Step 2 (see Supplementary Data for full set of result images): the 13 areas of the whole-brain networks shown to have significant difference in those with HH versus controls in their connectivity with the hypothalamus. They are shown over the standard MNI152 template and divided simply by general proximity onto six brain images for ease of viewing. HH, hypothalamic hamartoma; L, left; JLC, juxtapositional lobule cortex; NA, nucleus accumbens; NRA, nucleus retroambiguus; OTG, occipitotemporal gyrus; PAG, periaqueductal gray; PCG, posterior cingulate gyrus; PHG, parahippocampal gyrus; PT, planum temporal; SMG, supramarginal gyrus; R, right.

TABLE 2. SBCA RESULTS—CORTICAL AREAS OF HIGHEST TO LOWEST CONNECTIVITY DERANGEMENT

IC	Location	p	Previous method agreement
	Anterior 1/3 cingulate	0.0018	Yes
	Left occipitotemporal junction	0.0034	Yes
	Anterior 2/3 cingulate	0.0036	Yes
	Left parahippocampal gyrus, amygdala	0.0054	Yes
	Posterior cingulate	0.0084	Yes
	Periaqueductal gray, nucleus retroambiguus	0.0096	Yes
	Right putamen, thalamus	0.0236	Yes
	Right parahippocampal gyrus, amygdala	0.0292	Yes
	Left thalamus, operculum	0.0312	Yes
	Nucleus accumbens, caudate	0.0406	Yes
	Left hippocampus	0.0648	Yes

TABLE 2. (CONTINUED)

IC	Location	p	Previous method agreement
	Left planum temporal, supramarginal gyrus	0.2188	No
	Posterior bilateral thalami	0.3400	No

All 13 components identified by ICA ranked in order of highest connectivity increase detected by SBCA with the hypothalamus to lowest. The red checks denote agreement with prior ictal propagation studies. See Figure 2 for reference image number for full set of images provided in the Supplementary Data.

IC, identified component; ICA, independent component analysis; SBCA, seed-based correlation analysis.

areas with direct anatomical connection to the hypothalamus (Lauterbach et al., 2013) and identified along the initial seizure propagation pathway (Kokkinos et al., 2012) are the ventral septum and the nucleus retroambiguus in the pons, both of which were identified more broadly by fc measures in the nucleus accumbens area and brainstem-pons area, respectively.

Fc measures differentiated between those reported to be initial and remote-secondary seizure propagation pathway areas. Areas shown to be involved in more remote or secondary seizure propagation demonstrated significant connectivity differences in step 2, when comparing the whole-brain connectivity networks to those of normal individuals, but notably did not show significant connectivity disruptions directly with the HH itself in step 3. Namely, both the lateral frontal convexity and the planum temporal of the superior temporal gyrus do not have direct anatomical connections to the hypothalamus, and both were identified on interictal EEG-fMRI studies in the later propagation phase (Leal et al., 2009), which raises the possibility of fc-measures' ability to differentiate between areas of primary and more remote seizure propagation.

Hunyadi showed through simultaneous EEG-fMRI that an epileptogenic event is not necessary for rs-fMRI to identify the ictal source (Hunyadi et al., 2013). Hence, similar to metabolic changes affected by epileptogenic zones detectable by PET outside of the time of ictal phenomenon (Rastogi et al., 2008), it is reasonable to consider that fc measures designed to detect the gradation of the BOLD signal within areas functionally connected to the ictal driver are localizing with respect to the underlying pathology of the epilepsy.

Thus, our study is an initial evaluation of a potentially highly clinically applicable biomarker to possibly indirectly identify areas of maximal connectivity increase to the known ictal driver, which correspond to the areas of initial seizure propagation. It is unlikely that the results of this although small study were detected by chance as the method was purely data driven, was backed up by all of the prior invasive studies, and showed significant findings in only the areas previously identified.

Future directions

The least invasive most effective treatment of intractable epilepsy caused by HH is currently stereotactic laser ablation (STLA) of the HH (Wilfong and Curry, 2013). Understanding an individual's HH seizure propagation pathway through a noninvasive low-risk test would greatly aid in HH STLA disconnection planning, as often the lesion is too large for total ablation and/or demonstrates bilateral anatomical connections.

The first step toward this goal is demonstrated in this pilot group study, with all of the variables as well known as practically can be derived, including ictal source, ictal propagation pathway studies, and remote ictal propagation locations. In this study, only groupwise static connectivity disruption is considered. No immediate directionality can be concluded by this connectivity analysis technique, other than the groupwise local and remote areas identified that correlated with the other modalities' immediate and secondary areas along the seizure propagation pathway.

As a depth electrode study is not clinically indicated in HH, the next ethical step is large-scale individual analysis, examining fc-measure disruption in conjunction with prolonged-EEG study. Also needed is long-term postoperative observation on an individual basis with concurrent evaluation of the degree of cognitive abnormalities, behavioral problems, and hormonal abnormalities with the strength and location of the fc-linkage abnormality.

In this study, we specifically focused on detecting locations of maximal fc significant differences with the known HH ictal driver and correlated this with prior known areas of seizure prorogation. We did not differentiate the seizure onset zone from areas of initial propagation, which will be included in a future study. Data gathering is underway evaluating this technique to investigate seizures in which the anatomic nidus is unknown, as it may home in on areas of greatest connectivity derangement (the results of step 2). In epilepsy surgery candidates, this will provide a narrower menu of potential seizure foci, from which to query using the more invasive or hypothesis-driven techniques. In addition, if one or two ictal foci have been identified as possible ictal sources by other modalities, these areas can be further tested similarly to step 3. Thus these fc measures may provide possible propagation patterns, which can be correlated with other clinically available information, further weighing the evidence of seizure localization to one area. In addition, higher resolution data may yield more detailed results.

Development of such techniques to be evaluated in an intraoperative manner may allow surgeons to better understand if

disconnections from the seizure focus to the key areas' highest dysfunction have occurred, or do connections remain which are worth continued for intraoperative targeting.

Applicability of these fc measures to other pediatric patients with intractable epilepsy, such as those with diffuse cortical dysplasia or tuberous sclerosis, is currently being studied by us. In preliminary results of those with diffuse cortical dysplasia, ICA appears to identify an area contained within the dysplasia, but is generally larger than the smaller ictal focus identified by electrocorticographic means. A study evaluating postsurgical seizure freedom as predicted by fc measures is in progress. In addition, as with all children evaluated for epilepsy surgery at Texas Children's Hospital, data are being gathered in the tuberous sclerosis population. However, this population is extraordinarily variable and preliminary results are too speculative at this time.

Limitations

The controls of this study were not on medications, compared to those with HH, most of whom were on multiple antiepileptic drugs (AEDs). Effects of medications, especially combinations, on fcMRI-based measures are unknown. Two of 6 in the control group and 2 of 12 in the HH group received propofol, but it is unknown to what extent the combination of propofol with AEDs may influence connectivity measures.

This study was underpowered to separate subgroup differences based on age, as well as the differences in individuals with dominant left- versus right-sided HH. We acknowledge that an equal number of controls and subjects would have been preferable to our 1:2 ratio; the difference was due to constraints for such activities at a clinical facility, such as limited ability to add research patients into the clinical MRI schedule and limited funding. The total age range of the subject population was broad, potentially introducing age-related connectivity confounding that may not be present in a narrower age range group. The wide age range was due to HH being an extremely rare disorder, requiring participation of the entire clinical population of the facility to power the study.

Conclusions

(1) This study demonstrates the ability of connectivity analysis by combined ICA-SBCA to correctly identify the areas with highest connectivity derangement with the known seizure focus that correspond to the same areas of initial seizure propagation identified by prior modalities.

(2) The differentiation between initial and more remote areas of the prior established seizure propagation pathway was demonstrated through the level of connectivity with the known ictal driver.

(3) The identification of network disruption from the subcortical HH to large-scale neocortical networks shown in this study demonstrates the potential of fc measures and provides a model of analysis for other epileptic syndromes and network-based disease states.

Author Disclosure Statement

No competing financial interests exist.

References

Baroncini M, Jissendi P, Balland E, Besson P, Pruvo J, Francke J, et al. 2012. MRI atlas of the human hypothalamus. Neuroimage 59:168–180.

Beckmann CF, DeLuca M, Devlin JT, Smith SM. 2005. Investigations into resting-state connectivity using independent component analysis. Philos Trans R Soc Lond B Biol Sci 360:1001–1013.

Beckmann CF, Noble JA, Smith SM. 2000. Artefact detection in fMRI data using independent component analysis. Neuroimage 11:S614.

Beckmann CF, Smith SM. 2004. Probabilistic independent component analysis for functional magnetic resonance imaging. IEEE Trans Med Imaging 23:137–152.

Damoiseaux JS, Rombouts SA, Barkhof F, et al. 2006. Consistent resting-state networks across healthy subjects. Proc Natl Acad Sci U S A 103:13848–13853.

Delnooz CC, Pasman JW, Beckmann CF, van de Warrenburg BP. 2015. Altered striatal and pallidal connectivity in cervical dystonia. Brain Struct Funct 220:513–523.

Doria V, Beckmann CF, Arichi T, Merchant N, Groppo M, Turkheimer FE, et al. 2010. Emergence of resting state networks in the preterm human brain. Proc Natl Acad Sci U S A 107:20015–20020.

Filippini N, MacIntosh BJ, Hough MG, Goodwin GM, Frisoni GB, Smith SM, et al. 2009. Distinct patterns of brain activity in young carriers of the APOE-epsilon4 allele. Proc Natl Acad Sci U S A 106:7209–7214.

Fonov V, Evans AC, Botteron K, et al. 2011. Unbiased average age-appropriate atlases for pediatric studies. Neuroimage 54:313–327.

Gotman J, Pittau F. 2011. Combining EEG and fMRI in the study of epileptic discharges. Epilepsia 52(suppl 4):38–42.

Greve DN, Fischl B. 2009. Accurate and robust brain image alignment using boundary-based registration. Neuroimage 48:63–72.

Hunyadi B, Tousseyn S, Mijovic B, et al. 2013. ICA extracts epileptic sources from fMRI in EEG-negative patients: A retrospective validation study. PLoS One 8:e78796.

Jenkinson M, Bannister P, Brady M, Smith S. 2002. Improved optimization for the robust and accurate linear registration and motion correction of brain images. Neuroimage 17:825–841.

Jenkinson M, Beckmann CF, Behrens TE, Woolrich MW, Smith SM. 2012. FSL. Neuroimage 62:782–790.

Jenkinson M, Smith S. 2001. A global optimisation method for robust affine registration of brain images. Med Image Anal 5:143–156.

Kahane P, Ryvlin P, Hoffmann D, Minotti L, Benabid AL. 2003. From hypothalamic hamartoma to cortex: What can be learnt from depth recordings and stimulation? Epileptic Disord 5:205–217.

Kokkinos V, Zountsas B, Kontogiannis K, Garganis K. 2012. Epileptogenic networks in two patients with hypothalamic hamartoma. Brain Topogr 25:327–331.

Kuzniecky R, Guthrie B, Mountz J, et al. 1997. Intrinsic epileptogenesis of hypothalamic hamartomas in gelastic epilepsy. Ann Neurol 42:60–67.

Lauterbach EC, Cummings JL, Kuppuswamy PS. 2013. Toward a more precise, clinically-informed pathophysiology of pathological laughing and crying. Neurosci Biobehav Rev 37:1893.

Leal AJ, Monteiro JP, Secca MF, Jordao C. 2009. Functional brain mapping of ictal activity in gelastic epilepsy associated

with hypothalamic hamartoma: A case report. Epilepsia 50: 1624–1631.

Marcar VL, Schwarz U, Martin E, Loenneker T. 2006. How depth of anesthesia influences the blood oxygenation level-dependent signal from the visual cortex of children. AJNR Am J Neuroradiol 27:799–805.

Morgan VL, Abou-Khalil B, Rogers BP. 2015. Evolution of functional connectivity of brain networks and their dynamic interaction in temporal lobe epilepsy. Brain Connect 5: 35–44.

Murta T, Leal A, Garrido MI, Figueiredo P. 2012. Dynamic causal modelling of epileptic seizure propagation pathways: A combined EEG-fMRI study. Neuroimage 62: 1634–1642.

Nguyen D, Singh S, Zaatreh M, et al. 2003. Hypothalamic hamartomas: Seven cases and review of the literature. Epilepsy Behav 4:246–58.

Nichols TE, Holmes AP. 2002. Nonparametric permutation tests for functional neuroimaging: A primer with examples. Hum Brain Mapp 15:1–25.

O'Reilly JX, Beckmann CF, Tomassini V, Ramnani N, Johansen-Berg H. 2010. Distinct and overlapping functional zones in the cerebellum defined by resting state functional connectivity. Cereb Cortex 20:953–965.

Rastogi S, Lee C, Salamon N. 2008. Neuroimaging in pediatric epilepsy: A multimodality approach. Radiographics 28: 1079–1095.

Schrouff J, Perlbarg V, Boly M, Marrelec G, Boveroux P, Vanhaudenhuyse A, et al. 2011. Brain functional integration decreases during propofol-induced loss of consciousness. Neuroimage 57:198–205.

Smith SM, Fox PT, Miller KL, Glahn DC, Fox PM, Mackay CE, et al. 2009. Correspondence of the brain's functional architecture during activation and rest. Proc Natl Acad Sci U S A 106:13040–13045.

Smith SM, Nichols TE. 2008. Threshold-free cluster enhancement: Addressing problems of smoothing, threshold dependence and localisation in cluster inference. Neuroimage 44: 83–98.

Tagliazucchi E, Chialvo DR, Siniatchkin M, Amico E, Brichant JF, Bonhomme V, et al. 2016. Large-scale signatures of unconsciousness are consistent with a departure from critical dynamics. J R Soc Interface 13:20151027

Toulmin H, Beckmann CF, O'Muircheartaigh J, Ball G, Nongena P, Makropoulos A, et al. 2015. Specialization and integration of functional thalamocortical connectivity in the human infant. Proc Natl Acad Sci U S A 112:6485–6490.

Vanderby SA, Babyn PS, Carter MW, Jewell SM, McKeever PD. 2010. Effect of anesthesia and sedation on pediatric MR imaging patient flow. Radiology 256:229–237.

Wilfong AA, Curry DJ. 2013. Hypothalamic hamartomas: Optimal approach to clinical evaluation and diagnosis. Epilepsia 54(suppl 9):109–114.

Zarei M, Beckmann CF, Binnewijzend MA, Schoonheim MM, Oghabian MA, Sanz-Arigita EJ, et al. 2013. Functional segmentation of the hippocampus in the healthy human brain and in Alzheimer's disease. Neuroimage 66:28–35.

Address correspondence to:
Varina L. Boerwinkle
Department of Pediatric Neurology
Texas Children's Hospital
Baylor College of Medicine
6701 Fannin Street
CCC 1250
Houston, TX 77025

E-mail: varinab@bcm.edu